ELSEVIER

Electric Power Systems Research 37 (1996) 105–113

ELECTRIC POWER SYSTEMS RESEARCH

Spectral domain arcing fault recognition and fault distance calculation in transmission systems

Zoran M. Radojević, Vladimir V. Terzija *, Milenko B. Djurić

Faculty of Electrical Engineering, University of Belgrade, Bulevar Revalucije 73, PO Box 816, 11001 Belgrade, Yugoslavia

Received 1 September 1995; accepted 1 March 1996

Abstract

A new numerical algorithm for recognizing arcing faults for the purpose of automatic reclosing is presented. The fault distance can also be calculated using this algorithm. The solution for both symmetrical and unsymmetrical faults is given. A simple empirical arc voltage model is obtained through a table of numerical values. By means of computer simulation and laboratory testing it is shown that the algorithm can be used as an effective tool in transmission and distribution system protection.

Keywords: Power system protection; Autoreclosure; Arcing faults; Fault analysis; Harmonics

1. Introduction

As a large proportion of faults on a power system are of a temporary nature, the power system can be returned to its prefault state if the tripped circuit breakers are reclosed as soon as possible. Automatic reclosing can be high-speed, or it may be delayed. The term high-speed generally implies reclosing in times shorter than 1 second. Delayed reclosing usually operates in several seconds, or even minutes. Reclosing can be manual. It may be too slow for the purpose of restoring the power system to its prefault state when the system is in danger of becoming unstable.

The development of new microprocessor technology gave us an opportunity to control the automatic reclosing from a substation or reclosing computer. One of the main problems is to establish a concept for making a distinction between permanent and transient faults. It is known that reclosure on a permanent fault may aggravate the potential damage to the system and equipment. In this respect, some interesting concepts have been proposed in the past [1–4].

In Ref. [4] a new digital signal processing algorithm for arcing fault detection (for blocking automatic reclosing on lines with permanent faults) in transmission systems is presented. This algorithm can be applied only for three-phase symmetrical and double-phase faults. In this paper we provide an extension to the research presented in Ref. [4]. A new approach to modeling arc voltage is presented and a new solution for both unsymmetrical and symmetrical arcing fault detection. The algorithm is based on the simultaneous processing of the first and third voltage and current harmonics. They are used not only for arc voltage detection, but also for fault distance calculation. Thus, the algorithm can be used as an algorithm for fault location, too.

Numerous computer simulations have shown that the numerical algorithm developed can be used successfully as an effective tool for distinguishing between permanent and transient faults. The results of laboratory tests are also given, confirming the results obtained through computer simulations.

2. Essential properties of the arc

The correlation of voltage and current in an electric arc is entirely different from that in solid conductors. Whereas in metals the voltage is proportional to the current ($v = Ri$), the voltage between the electrodes of a burning arc decreases with rising current to a limiting value and again increases if the current diminishes.

If voltage and current are measured at an arc, distorted curve shapes are found depending on the type of

* Corresponding author. E-mail Eterzija@UBBG.ETF.BG.AC.YU.

PII S0378-7796(96)01044-9

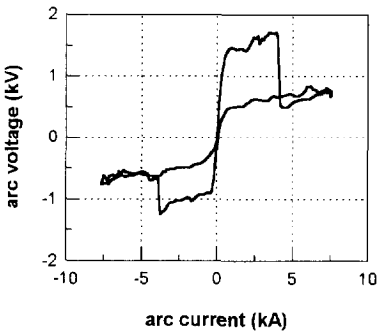

Fig. 1. Arc voltage–current characteristic.

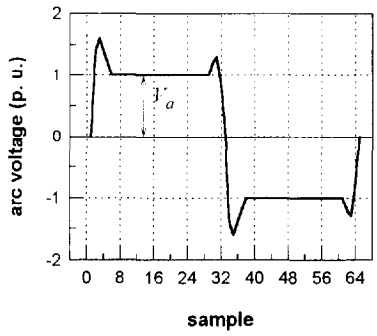

Fig. 2. Arc voltage wave shape.

arc gas, the material of the electrodes, and the frequency of the current. The initial breakdown of the gap between the electrodes requires a high ignition voltage at zero current. The subsequently increasing current rapidly augments the conductance of the air so that the arc voltage gradually decreases. This deviating behavior, compared with metals, is due to different types of current transport in an arc [5]. It results in a nonlinear arc voltage–current characteristic, depicted in Fig. 1 (the characteristic was obtained under laboratory conditions at Forschungsgemeinschaft für Hochspannung- und Hochstromtechnik e.V. (FGH), Mannheim, Germany, in 1992). Such a characteristic is typical for long arcs in free air, in which we are interested.

From a modeling point of view, the arc voltage could be represented by a nonlinear differential equation [6], or through current dependent models [7]. It can also be represented by piecewise arc voltage–current characteristics [8].

In this paper, the arc voltage wave shape was defined numerically on the basis of a great number of arc voltage records obtained in the high-voltage laboratory of FGH in 1992. The arc voltage model given in Table 1 and Fig. 2 is accepted. Table 1 gives only a normalized positive half cycle of the arc voltage model with arc voltage amplitude $V_a = 1$ p.u. It is assumed that the sign of these values is determined by the sign of the arc current.

The values of V_a are obtained from the product of the arc voltage gradient (over the range of currents from 100 A to 20 kA the average arc voltage gradient lies between 12 and 15 V/cm [9]) and the length of the path, i.e. the flashover length of a suspension insulator string or the flashover length between conductors.

The arc model given in Table 1 has an important feature in the spectral domain: it can be represented by a Fourier series containing odd sine components only, as follows:

$$v_a(t) = \sum_{h=1}^{\infty} k_h V_a \sin(h\omega t) \tag{1}$$

where $h = 1, 3, 5, 7, \ldots$ is the harmonic order, ω is the fundamental radian frequency and k_h is the coefficient of the hth harmonic. Using the fast Fourier transform (FFT) algorithm it is easy to obtain coefficients k_h for the accepted arc voltage model. These coefficients are given in Table 2.

In comparison with other models, the advantage of the arc voltage representation through the sequence of numerical values is its flexibility. Various wave shapes can be created and the corresponding coefficients k_h calculated, depending on the modeling application.

If the first and the third harmonics of the arc voltage are obtained from this set of data, the value of the arc voltage amplitude V_a can be estimated and the distance from the line terminal to the fault calculated. This is shown in the next section.

3. Arc voltage amplitude and fault distance calculation

The amplitude of the hth harmonic of the arc voltage can be expressed through the relation

$$V_{ah} = k_h V_a \tag{2}$$

where V_{ah} is the amplitude of the hth harmonic of the arc voltage. From Eq. (2) we obtain

$$V_{a1} = k_1 V_a = 1.3 V_a \text{ and } V_{a3} = k_3 V_a = 0.497 V_a \tag{3}$$

The arc voltage wave shape is in phase with the fault arc current. This means that the phase of the first harmonic of the arc voltage is the same as the phase of the first arc current harmonic. In addition, the phase of the third harmonic of the arc voltage is three times greater than the phase of the first harmonic of the arc voltage. Thus,

Table 1
Arc voltage model

Sample	1	2	3	4	5	6	7	...	28	29	30	31	32
v_a (p.u)	0	1.4	1.6	1.4	1.2	1	1	...	1	1	1.2	1.3	0.8

Table 2
Coefficients of the hth harmonics of the arc voltage

h	1	3	5	7	9
k_h	1.3	0.497	0.35	0.275	0.21

$$\underline{V}_{a1} = \underline{k}_1 V_a \tag{4}$$

and

$$\underline{V}_{a3} = \underline{k}_3 V_a \tag{5}$$

where $\underline{V}_{a1}$ and $\underline{V}_{a3}$ are phasors of the first and third harmonics of the arc voltage, $\underline{k}_1 = k_1 \angle \phi$ and $\underline{k}_3 = k_3 \angle (3\phi)$, where ϕ is the phase of the first harmonic of the arc current ($\underline{I}_1 = I_1 \angle \phi$). Eqs. (4) and (5) are the basis for further algorithm development.

It is practically impossible to measure arc voltage, since the fault has an arbitrary location on the line. The idea given in this paper is to calculate the arc voltage amplitude from the line terminal voltage and current signals obtainable as uniformly digitized quantities at one of the line terminals. In the case of arcing faults, voltages and currents at the line terminals contain harmonics as well. The distortion of these waves depends on the fault distance and the arc voltage amplitude. Through spectral analysis it can be concluded that the line terminal voltages and currents contain harmonics induced by the arc voltage, particularly the odd components. These amplitudes are not comparable to the fundamental harmonic amplitude, but in spite of that they are recognizable and measurable [4].

One of the obvious ways in which arc voltage harmonics can be calculated is to analyze the line equivalent circuit depicted in Fig. 3. In this circuit all variables have radian frequency $h\omega$ and all line parameters are calculated in terms of $h\omega$. By using the FFT, the corresponding harmonic components $\underline{V}_h$ and $\underline{I}_h$ can be calculated. From the line equivalent circuit depicted in Fig. 3 the hth arc voltage harmonic can be expressed as follows:

$$\underline{V}_{ah} = \underline{V}_h(1 + \underline{Y}_h \underline{Z}_h l^2) - \underline{Z}_h l \underline{I}_h \tag{6}$$

where $\underline{Z}_h$ (Ω/km) $= R(h\omega) + jh\omega L(h\omega)$ and $\underline{Y}_h$ (S/km) $= jh\omega C(h\omega)$ are the frequency dependent line impedance and admittance, respectively, and l (km) is the fault distance from the observed line terminal.

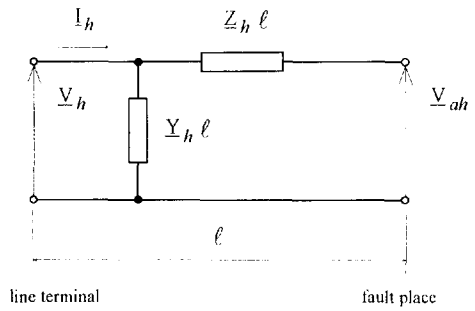

Fig. 3. Line equivalent circuit.

3.1. Solution for three-phase and double-phase faults

Using Eqs. (5) and (6) the following relations can be written:

$$\underline{k}_1 V_a = \underline{V}_1(1 + \underline{Y}_1 \underline{Z}_1 l^2) - \underline{Z}_1 l \underline{I}_1 \tag{7}$$

$$\underline{k}_3 V_a = \underline{V}_3(1 + \underline{Y}_3 \underline{Z}_3 l^2) - \underline{Z}_3 l \underline{I}_3 \tag{8}$$

From Eqs. (7) and (8) a direct expression for l is obtained:

$$l = \frac{\underline{V}_1(1 + \underline{Y}_1 \underline{Z}_1 l^2) - \underline{K}\,\underline{V}_3(1 + \underline{Y}_3 \underline{Z}_3 l^2)}{\underline{Z}_1 \underline{I}_1 - \underline{K}\,\underline{Z}_3 \underline{I}_3} \tag{9}$$

where

$$\underline{K} = \frac{\underline{k}_1}{\underline{k}_3} = \frac{k_1 \angle \phi}{k_3 \angle (3\phi)} = 2.6157 \angle (-2\phi)$$

The value of $|\underline{K}|$ ($= 2.6157$) is determined by the arc voltage model assumed (see Table 1). For other arc voltage shapes the new values can be obtained by using the FFT (i.e. by determining the arc voltage amplitude and phase spectra), so $|\underline{K}|$ can be 'tuned' to the actual application. Through the computer simulation it was deduced that the choice of $|\underline{K}|$ does not essentially affect the algorithm's accuracy.

Eq. (9) represents a quadratic equation in terms of l. The value of l can be directly determined by solving the quadratic equation with complex coefficients. To simplify the calculation of l, it was noticed that $\underline{Y}_1 \underline{Z}_1 l^2 \ll 1$ and $\underline{Y}_3 \underline{Z}_3 l^2 \ll 1$. Thus, in the first step l can be calculated directly from Eq. (9) under the assumption that $l^2 = 0$. In the second step l can be calculated directly from Eq. (9), without neglecting terms with l^2, making a correction for the first calculated value of l. After calculating l it is simple to calculate V_a using either Eq. (7) or Eq. (8). Both the calculated values of l and V_a are practically real values, so the small imaginary components can be neglected.

The new digital algorithm for arc voltage amplitude and fault distance calculation can be subdivided into the following steps:

Step 1. Acquisition of input signals block (line terminal voltages and currents)
Step 2. Determination of the first and third harmonics of input signals
Step 3. Fault distance calculation using Eq. (9)
Step 4. Arc voltage amplitude calculation using Eqs. (7) and (8)

Step 5. Decision as to whether the fault is with arc (transient fault) or without arc (permanent fault)

The algorithm presented can be used directly for three-phase symmetrical and double-phase faults (i.e. for earthless faults). For three-phase faults, Eqs. (7)–(9) require phase voltages and currents. For double-phase faults, Eqs. (7)–(9) require phase-to-phase voltages and a difference between phase currents.

3.2. Solution for the unsymmetrical faults

Using the symmetrical component approach and the line equivalent circuit depicted in Fig. 3 for the positive-, negative- and zero-sequence components of the voltages and currents (see Appendix), it is easy to extend Eqs. (7) and (8) for single phase-to-earth and double phase-to-earth faults, as follows:

$$\underline{k}_1 V_a = \underline{V}_1(1 + \underline{Y}_1\underline{Z}_1 l^2) + \underline{V}_{10}(\underline{Y}_{10}\underline{Z}_{10} - \underline{Y}_1\underline{Z}_1)l^2 - \underline{Z}_1 l(\underline{I}_1 + \underline{K}_1\underline{I}_{10}) \quad (10)$$

$$\underline{k}_3 V_a = \underline{V}_3(1 + \underline{Y}_3\underline{Z}_3 l^2) + \underline{V}_{30}(\underline{Y}_{30}\underline{Z}_{30} - \underline{Y}_3\underline{Z}_3)l^2 - \underline{Z}_3 l(\underline{I}_3 + \underline{K}_3\underline{I}_{30}) \quad (11)$$

where $\underline{K}_1 = (\underline{Z}_{10} - \underline{Z}_1)/\underline{Z}_1$ and $\underline{K}_3 = (\underline{Z}_{30} - \underline{Z}_3)/\underline{Z}_3$ are compensatory coefficients, $\underline{Z}_{10}$ and $\underline{Z}_{30}$ are the line zero-sequence impedances for the first and the third harmonics, $\underline{I}_{10}$ and $\underline{I}_{30}$ are the first and third harmonics of the zero-sequence current, $\underline{V}_{10}$ and $\underline{V}_{30}$ are the first and third harmonics of the zero-sequence voltage, and $\underline{Y}_{10}$ and $\underline{Y}_{30}$ are the line zero-sequence admittances for the first and third harmonics.

Next, by replacing V_a from Eq. (11) in Eq. (10) one obtains

$$l = \frac{\underline{V}_1(1 + \underline{Y}_1\underline{Z}_1 l^2) - \underline{K}\,\underline{V}_3(1 + \underline{Y}_3\underline{Z}_3 l^2)}{\underline{Z}_1(\underline{I}_1 + \underline{K}_1\underline{I}_{10}) - \underline{K}\,\underline{Z}_3(\underline{I}_3 + \underline{K}_3\underline{I}_{30})} + \frac{\underline{V}_{10}(\underline{Y}_{10}\underline{Z}_{10} - \underline{Y}_1\underline{Z}_1) - \underline{K}\,\underline{V}_{30}(\underline{Y}_{30}\underline{Z}_{30} - \underline{Y}_3\underline{Z}_3)}{\underline{Z}_1(\underline{I}_1 + \underline{K}_1\underline{I}_{10}) - \underline{K}\,\underline{Z}_3(\underline{I}_3 + \underline{K}_3\underline{I}_{30})} l^2 \quad (12)$$

High-voltage and extra-high-voltage lines with ground wires have parameters such that the differences $\underline{Y}_{10}\underline{Z}_{10} - \underline{Y}_1\underline{Z}_1$ and $\underline{Y}_{30}\underline{Z}_{30} - \underline{Y}_3\underline{Z}_3$ are negligible. This means that the second addend in Eq. (12) can be neglected, so Eq. (12) can be written as

$$l = \frac{\underline{V}_1(1 + \underline{Y}_1\underline{Z}_1 l^2) - \underline{K}\,\underline{V}_3(1 + \underline{Y}_3\underline{Z}_3 l^2)}{\underline{Z}_1(\underline{I}_1 + \underline{K}_1\underline{I}_{10}) - \underline{K}\,\underline{Z}_3(\underline{I}_3 + \underline{K}_3\underline{I}_{30})} \quad (13)$$

For short lines (up to 150 km), Eq. (13) can be simplified as

$$l = \frac{\underline{V}_1 - \underline{K}\,\underline{V}_3}{\underline{Z}_1(\underline{I}_1 + \underline{K}_1\underline{I}_{10}) - \underline{K}\,\underline{Z}_3(\underline{I}_3 + \underline{K}_3\underline{I}_{30})} \quad (14)$$

After calculating l, V_a can be obtained directly from Eq. (10).

The algorithm presented was tested extensively through computer simulated and laboratory tests, as described in Section 4.

4. Computer simulated tests

The electromagnetic transient program (EMTP), as developed at the University of Kaiserslauten [10], was used to generate the sample data required. The schematic diagram of the 400 kV power system on which the tests are provided is shown in Fig. 4. Here $v(t)$ and $i(t)$ are the digitized voltages and currents, D is the line length and l the fault distance. The line parameters selected were $D = 100$ km, $R = 6.5\ \Omega$, $L = 0.0941$ H, $L_0 = 0.2823$ H, $C = 610$ nF and $C_0 = 373$ nF.

4.1. Dynamic tests on the 400 kV power system

Faults are identified as close-in ($l = 10$ km) and remote ($l = 80$ km), measured from the left-hand line end. The following two cases were analyzed: (a) $l = 10$ km, instance of fault inception 0.035 s (case 1), and (b) $l = 80$ km, instance of fault inception 0.030 s (case 2). Figs. 5 and 6 (cases 1 and 2) show the left-hand line terminal faulted-phase voltages and currents, sampled with the sampling frequency 6400 Hz (128 samples/0.02 s) for single-phase faults with arc ($V_a = 3500$ V was the exact value). The equivalent tests without arc ($V_a = 0$) are also provided.

By processing the generated voltages and currents for cases 1 and 2 with arc, the arc voltages and fault distances calculated via the algorithm presented are depicted in Figs. 7 and 8, respectively. All relevant curves before, during and after the instance of fault inception are depicted in both figures so the complete convergence process can be viewed. During the transient process some estimates reach large transient values and the graph scaling is not appropriate for close inspection of the values obtained. Therefore, the next diagrams are enlarged in order to depict only the final

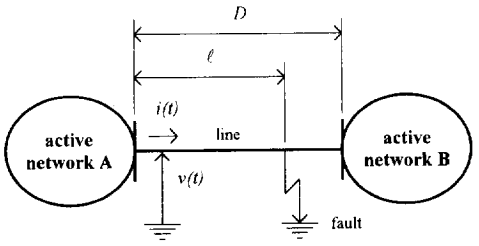

Fig. 4. Test power system.

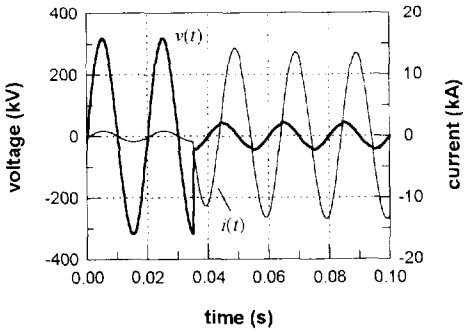

Fig. 5. Faulted-phase line terminal voltage and current (case 1).

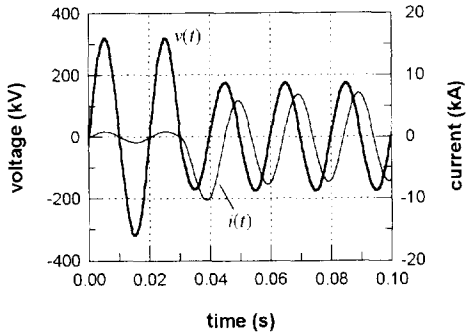

Fig. 6. Faulted-phase line terminal voltage and current (case 2).

unknown values, and the large values obtained during the convergence period are omitted (Figs. 9–12).

When considering the speed of the arc voltage and fault distance calculation (the algorithm convergence), it can be concluded from Figs. 7 and 8 that it is fast enough from the autoreclosure point of view. Reliable information about the fault type can be obtained approximately 30 ms after fault inception (note that the instances of fault inception are 0.035 and 0.030 s, respectively).

Calculated arc voltages are depicted in Figs. 9 and 10 for cases 1 and 2, respectively, with and without arc, while the calculated distances are shown in Figs. 11 and 12. The scaling in all figures is selected so as to present only the values finally obtained. The complete conver-

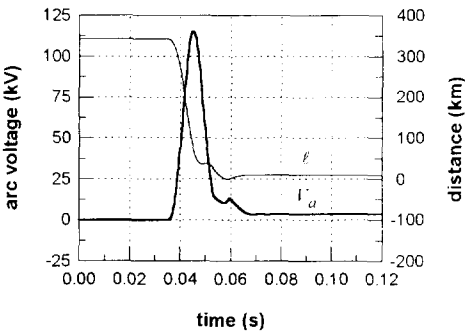

Fig. 7. Calculated values for case 1 (fault with arc).

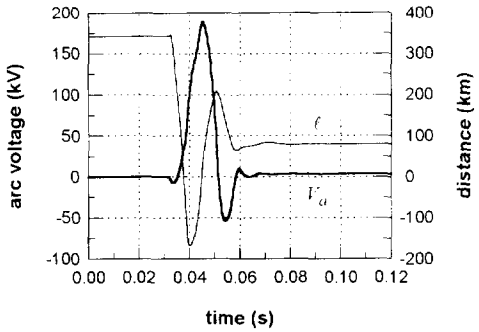

Fig. 8. Calculated values for case 2 (fault with arc).

gence periods for all cases are similar to the graphs presented in Figs. 7 and 8.

The tests presented were performed with the network fed only from one side, which is a typical configuration for distribution systems. In these tests the initial assumption that "arc current, arc voltage and line terminal current are in phase" was satisfied, so the results obtained were quite correct. The above-mentioned assumption is not satisfied when a network fed from two sides is considered, because the arc current (i.e. fault current) is a sum of the left and right line terminal currents (see Fig. 13), resulting in the terminal currents not being in phase with the arc current and arc voltage

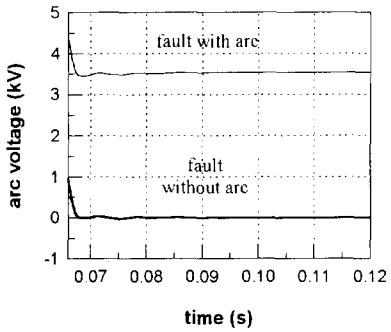

Fig. 9. Calculated arc voltages for case 1.

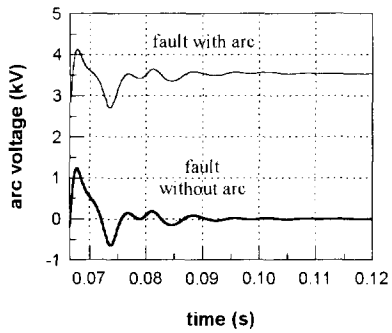

Fig. 10. Calculated arc voltage for case 2.

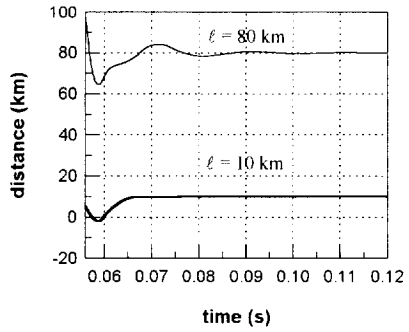

Fig. 11. Calculated fault distances for case 1 (faults without arc).

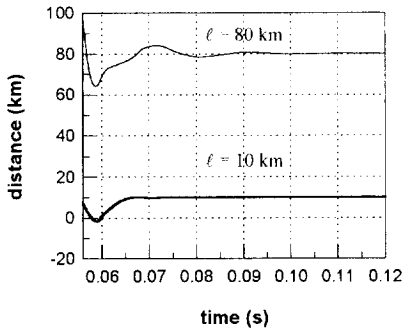

Fig. 12. Calculated fault distances for case 2 (faults with arc).

(arc current and arc voltage are always in phase due to the nature of the arc).

In Fig. 13, v, R and L are voltage, resistance and inductance, respectively; indices A and B denote the left and the right sides. In order to investigate the influence of phase shift between terminal current and arc current on the algorithm's accuracy, the following test was performed: the phase shift ϑ between the generator voltages of the active networks A and B was changed. The left-hand voltage was selected to be the reference voltage with zero phase shift. The numerical algorithm was tested by changing the phase shift ϑ_B (in the range 0–20°) of the right-hand generator network. Two sets of tests were performed with arc voltage $V_a = 1000$ V. In the first set, close-in faults ($l = 80$ km) were analyzed. For the calculated distance l and arc voltage amplitude V_a, the relative errors ρ (in %) are shown in Table 3. As the real phase shift ϑ is less than 10°, from Table 3 it can be concluded that the algorithm presented retains the satisfactory accuracy. Thus, the algorithm can be implemented not only for radial

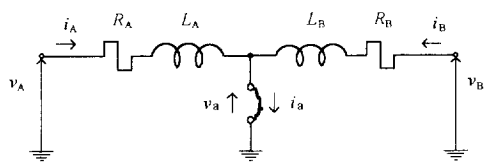

Fig. 13. Arc current fed from both line sides.

Table 3
Sensitivity analysis on the phase shift between generators A and B ($V_a = 1000$ V)

ϑ_B (deg)	$l = 10$ km		$l = 80$ km	
	ρ_l (%)	ρ_{V_a} (%)	ρ_l (%)	ρ_{V_a} (%)
0.0	−1.16	1.40	−1.37	1.80
2.5	−1.16	1.40	−1.37	1.80
5.0	−1.16	1.40	−1.44	1.80
7.5	−1.18	1.39	−1.49	0.58
10.0	−1.45	1.80	−1.50	−2.90
12.5	−1.46	1.84	−1.51	−2.92
15.0	−1.47	1.80	−1.56	−8.50
17.5	−1.74	0.10	−1.57	−8.52
20.0	−1.80	0.10	−1.61	−16.0

networks, but also for networks fed from both sides. In addition, it was proved that the fault distance calculation does not depend on whether the line is fed from both sides, or not.

Since the arc voltage wave shape depicted in Fig. 2 is only an approximation of the real arc voltage waveform, in the following test an example is shown where the arc voltage took a more realistic shape [10] (Fig. 14). Satisfactory output values (fault distance and arc voltage) were obtained, and are shown in Fig. 14. In the test the exact fault distance was $l = 50$ km.

Finally, the algorithm's sensitivity to harmonics generated from other power system nonlinear sources is investigated. In the tests the exact values were $V_a = 3500$ V and $l = 50$ km. As only first and third harmonics are taken into account, other harmonics cannot affect the algorithm's accuracy. This is proved through the test in which the 7th harmonic was artificially injected by generator A in an unrealistic amount of 0.2 p.u. The input line terminal voltage and current are depicted in Fig. 15, and the arc voltage amplitude V_a and distance l in Fig. 16.

The next test shows that the algorithm is not only sensitive to the presence of the 3rd harmonic (which is

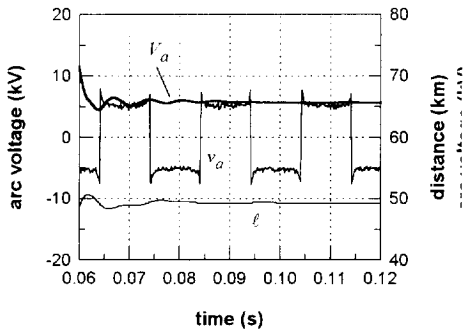

Fig. 14. Arc voltage waveform and its estimated amplitude V_a.

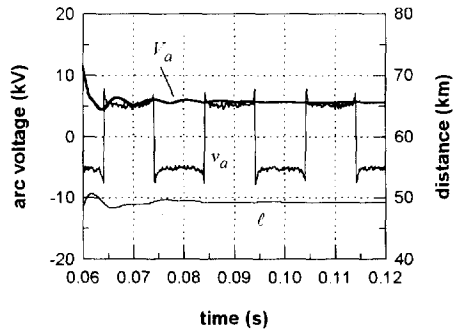

Fig. 15. Input voltage and current in the test with the 7th harmonic.

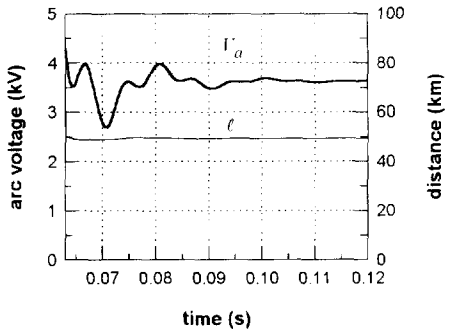

Fig. 16. Calculated algorithm outputs in the test with the 7th harmonic.

an input to the algorithm), but also to the presence of a combination of harmonics injected by other harmonic sources. First, the 3rd harmonic (0.2 p.u.) was injected from generator A. Then a combination of the 3rd, 5th and 7th harmonics (all 0.2 p.u.) was injected by the same generator. The algorithm inputs and outputs are depicted in Figs. 17–20, respectively.

It is noticed that in all cases the calculated fault distance l and arc voltage amplitude V_a are correctly calculated, proving that the new algorithm is not sensitive to the harmonics generated by other power system sources.

5. Laboratory tests

In order to check the validity of the presented algorithm, data obtained at FGH were used. Voltage $v(t)$, current $i(t)$ and arc voltage $v_a(t)$ were digitized by the laboratory test circuit depicted in Fig. 21. The arc between iron rod electrodes was initiated by means of a fuse wire when switch S in Fig. 21 was closed. The distance between the electrodes was selected to be 60 cm. The data were digitized using a modern transient recorder with a sampling frequency of 10.417 kHz. The input voltage $v(t)$ and current $i(t)$ are depicted in Fig. 22, the arc voltage $v_a(t)$ and its estimated amplitude V_a in Fig. 23. The arc length, proportional to the arc voltage, is shown in Fig. 23 with a scale in cm (it was assumed that the arc voltage gradient is about 12.5 V/cm).

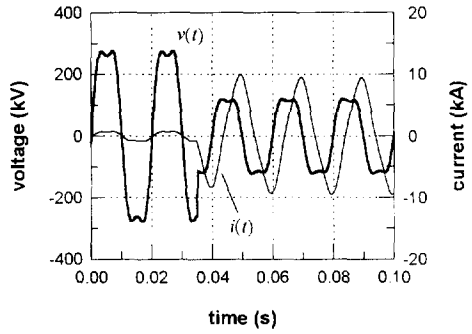

Fig. 17. Input voltage and current in the test with the 3rd harmonic.

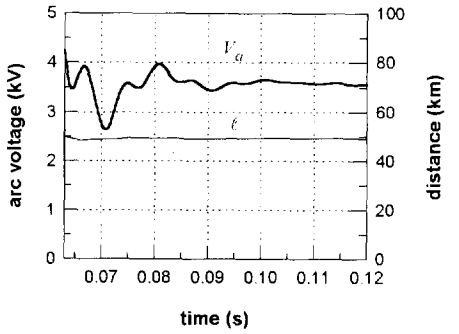

Fig. 18. Calculated algorithm outputs in the test with the 3rd harmonic.

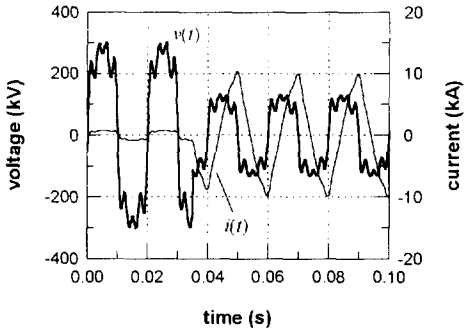

Fig. 19. Input voltage and current in the test with the 3rd, 5th and 7th harmonics.

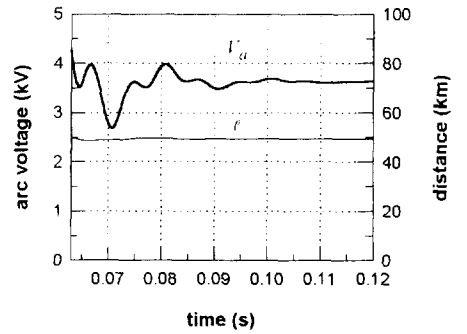

Fig. 20. Calculated algorithm outputs in the test with the 3rd, 5th and 7th harmonics.

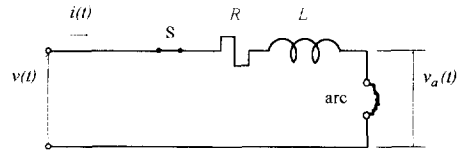

Fig. 21. Laboratory test circuit.

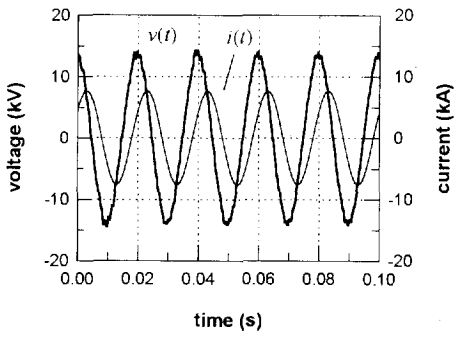

Fig. 22. Input voltage and current in the laboratory tests.

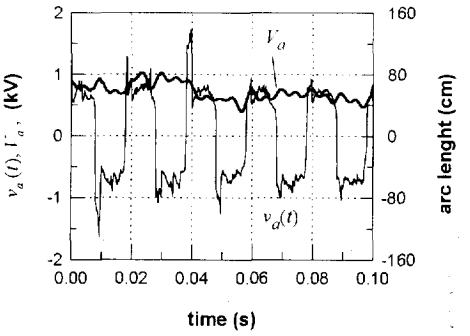

Fig. 23. Arc voltage waveform, amplitude and length calculated in laboratory testing.

From the laboratory tests presented in this section, as well as from the calculated arc voltages depicted in Fig. 23, it can be concluded that the new algorithm can distinguish faults with and without arc, i.e. it can precisely calculate the arc voltage by processing the line terminal voltages and currents.

6. Conclusions

A new numerical algorithm for blocking automatic reclosing of lines with permanent symmetrical or unsymmetrical faults is presented. It can also be used for fault distance calculation. A new approach to modeling arc voltage is given. The algorithm was derived by processing line terminal voltages and currents during the period between fault inception and fault clearance. It is based on spectral analysis of the input signals and on the utilization of the first and third harmonics. The algorithm was successfully tested with data obtained through computer simulation and data recorded in laboratory tests. The algorithm's insensitivity to harmonics originating from other sources was proven.

Acknowledgements

The authors wish to thank Professor D. Nelles (TU Kaiserslautern, Germany) for his helpful advice and suggestions during the early phases of this work. FGH Mannheim is gratefully acknowledged for data used in laboratory testing.

Appendix A

Using the symmetrical components approach and the line equivalent circuit of Fig. 3 for positive-, negative- and zero-sequence components of the first harmonic of the line terminal voltages and currents it is possible to write the following equations:

$$\underline{V}_{a1p} = \underline{V}_{1p}(1 + \underline{Y}_1\underline{Z}_1 l^2) - \underline{Z}_1\underline{I}_{1p} \quad \text{(A1)}$$

$$\underline{V}_{a1n} = \underline{V}_{1n}(1 + \underline{Y}_1\underline{Z}_1 l^2) - \underline{Z}_1 l\underline{I}_{1n} \quad \text{(A2)}$$

$$\underline{V}_{a10} = \underline{V}_{10}(1 + \underline{Y}_{10}\underline{Z}_{10} l^2) - \underline{Z}_{10} l\underline{I}_{10} \quad \text{(A3)}$$

where p, n and 0 are indices for positive-, negative- and zero-sequence components and $\underline{Z}_{1p} = \underline{Z}_{1n} = \underline{Z}_1$.

By adding Eqs. (A1)–(A3) one obtains

$$\begin{aligned}\underline{V}_{a1p} + \underline{V}_{a1n} + \underline{V}_{a10} = \underline{V}_{a1} = \underline{k}_1 V_a \\ = \left(\underline{V}_{1p} + \underline{V}_{1n} + \underline{V}_{10}\frac{1 + \underline{Y}_{10}\underline{Z}_{10} l^2}{1 + \underline{Y}_1\underline{Z}_1 l^2}\right) \\ \times (1 + \underline{Y}_1\underline{Z}_1 l^2) \\ - \underline{Z}_1 l\left(\underline{I}_{1p} + \underline{I}_{1n} + \underline{I}_{10}\frac{\underline{Z}_{10}}{\underline{Z}_1}\right)\end{aligned} \quad \text{(A4)}$$

Eq. (10) follows directly from Eq. (A4). By replacing index 1 with 3 in Eq. (A4) it follows that

$$\begin{aligned}\underline{V}_{a3p} + \underline{V}_{a3n} + \underline{V}_{a30} = \underline{V}_{a3} = \underline{k}_3 V_a \\ = \left(\underline{V}_{3p} + \underline{V}_{3n} + \underline{V}_{30}\frac{1 + \underline{Y}_{30}\underline{Z}_{30} l^2}{1 + \underline{Y}_3\underline{Z}_3 l^2}\right) \\ \times (1 + \underline{Y}_3\underline{Z}_3 l^2) \\ - \underline{Z}_3 l\left(\underline{I}_{3p} + \underline{I}_{3n} + \underline{I}_{30}\frac{\underline{Z}_{30}}{\underline{Z}_3}\right)\end{aligned} \quad \text{(A5)}$$

Eq. (11) follows directly from Eq. (A5).

References

[1] Y. Ge, F. Sui and Y. Xiao, Prediction methods for preventing single-phase reclosing on permanent fault, *IEEE Trans. Power Delivery*, *4* (1) (1989) 114–121.

[2] R.K. Aggarwal, A.T. Johns, Y.H. Song, R.W. Dunn and D.S. Fitton, Neural-network based adaptive single-pole autoreclosure technique for EHV transmission systems, *IEEE Proc. Gener. Transm. Distrib.*, *141* (2) (1994) 155–160.

[3] M.B. Djurić, V.V. Terzija and L.A. Škokljev, Tansmission line arcing faults recognition from the voltage signal, *Proc. 11th Power Systems Computation Conf. (PSCC), Avignon, France, 1993*, Vol. II, pp. 1037–1040.

[4] M.B. Djurić and V.V. Terzija, A new approach to the arcing faults detection for autoreclosure in transmission systems, *IEEE Trans. Power Delivery*, *10* (4) (1995) 1793–1798.

[5] R. Rüdenberg, *Elektrische Schaltvorgänge in geschlossenen Stromkreisen von Starkstromanlagen*, Springer, Berlin, 1953.

[6] M. Kizilcay and K.-H. Koch, Numerical fault arc simulation based on power arc tests, *Eur. Trans. Electr. Power Eng. (ETEP)*, *4* (3) (1994) 177–185.

[7] V. Terzija and D. Nelles, Parametrische Modelle des Lichtbogens und Parameterschätzung auf Grund der simulierten und echten Daten, *TB-183/93*, Technical University of Kaiserslautern, Germany, 1993.

[8] A.T. Johns, R.K. Aggarwal and Y.H. Song, Improved technique for modeling fault arc on faulted EHV transmission systems, *IEE Proc. Gener. Transm. Distrib.*, *141* (2) (1994) 148–154.

[9] A.S. Maikapar, Extinction of an open electric arc, *Elektrichestvo*, *4* (1960) 64–69.

[10] D. Lönard, R. Simon and V. Terzija, Simulation von Netzmodellen mit zweiseitiger Einspeisung zum Test von Netzschutzeinrichtungen, *TB-157/92*, University of Kaiserslautern, Germany, 1992.